THE JOURNAL OF BIOLOGICAL CHEMISTRY VOL. 284, NO. 3, pp. 1620–1627, January 16, 2009

Modulation of Cell Motility by Spatial Repositioning of Enzymatic ATP/ADP Exchange Capacity*[S]

Received for publication, September 9, 2008, and in revised form, November 12, 2008 Published, JBC Papers in Press, November 12, 2008, DOI 10.1074/jbc.M806974200

Remco van Horssen[‡1], Edwin Janssen[‡1,2], Wilma Peters[†‡], Loes van de Pasch[‡], Mariska M. te Lindert[‡], Michiel M. T. van Dommelen[‡], Peter C. Linssen[§], Timo L. M. ten Hagen[¶], Jack A. M. Fransen[‡], and Bé Wieringa[‡3]

From the [‡]Department of Cell Biology, Nijmegen Center for Molecular Life Sciences and [§]Department of Hematology, Radboud University Nijmegen Medical Center, 6500 HB Nijmegen, The Netherlands and the [¶]Department of Surgical Oncology, Erasmus MC, 3000 DR Rotterdam, The Netherlands

ATP is the "principal energy currency" in metabolism and the most versatile small molecular regulator of cellular activities. Although already much is known about the role of ATP in fundamental processes of living systems, data about its compartmentalization are rather scarce, and we still have only very limited understanding of whether patterns in the distribution of intracellular ATP concentration ("ATP inhomogeneity") do exist and have a regulatory role. Here we report on the analysis of coupling of local ATP supply to regulation of actomyosin behavior, a widespread and dynamic process with conspicuous high ATP dependence, which is central to cell shape changes and cell motility. As an experimental model, we use embryonic fibroblasts from knock-out mice without major ATP-ADP exchange enzymes, in which we (re)introduce the ATP/ADP exchange enzyme adenylate kinase-1 (AK1) and deliberately manipulate its spatial positioning by coupling to different artificial location tags. By transfection-complementation of AK1 variants and comparison with yellow fluorescent protein controls, we found that motility and spreading were enhanced in cells with AK1 with a focal contact guidance tag. Intermediary enhancement was observed in cells with membrane-targeted or cytosolic AK1. Use of a heterodimer-inducing approach for transient translocation of AK1 to focal contacts under conditions of constant global AK1 activity in the cell corroborated these results. Based on our findings with these model systems, we propose that local ATP supply in the cell periphery and "on site" fuelling of the actomyosin machinery, when maintained via enzymes involved in phosphoryl transfer, are codetermining factors in the control of cell motility.

Maintenance of adequate ATP supply is of crucial importance for the mechanisms of structural remodeling in cells with high shape plasticity, especially under high energy-demanding circumstances (1). During processes like cell motility or phagocytosis, the cell movement and cellular shape changes require active restructuring of the actin cytoskeleton. By spatially controlled polymerization of ATP-bound G-actin monomers to the plus end of growing actin filaments and formation of multiple branches, a dense network is built, which is called the actin cortex, based on its specific localization within the cell (2). In this network, ATP hydrolysis and release of P_i drive actin filament dynamics by modulating filament stability and determine nucleotide-dependent filament conformation and interaction(s) with regulatory actin-binding proteins (3). Furthermore, force generation needed for contraction and cell movement is controlled by myosin and nonmuscle myosin ATPases (4), and also upstream signaling, involving small GTPases, is contingent upon nucleotide exchange (5). Taken together, actomyosin dynamics is overall an energy-demanding process, directly coupled to ATP availability.

Indeed, actomyosin-based processes may consume a major fraction of cellular energy (6). Moreover, the coupling between global ATP supply and cytoskeletal dynamics seems reciprocal, because in tissues under ischemia, actomyosin activity is set in accordance with ATP availability (7).

Against this background, it is an important question whether ATP-to-actomyosin coupling also acts at the subcellular level and could have a role in spatial control of cell dynamics. Studies in *Physarum polycephalum* pointed for the first time to a role for patterns in distribution of intracellular ATP concentration in the coordination of cell motility behavior, probably via effects on cytoskeletal dynamics (8). Our recent work on the process of phagocytosis pointed in the same direction and gave new insight into how ATP production in cellular microdomains, mediated by brain-type creatine kinase-driven phosphotransfer, relates to local coordination of actin-based cell shape remodeling (9). Despite this progress, our understanding of the significance of local distribution of ATP/ADP pools (*i.e.* inhomogeneity in intracellular [ATP]/[ADP]) and the diverse molecular mechanisms that contribute to patterning in distribution is still very limited.

Here we study the supposed regulatory and codetermining role of ATP/ADP supply in microdomains further by analyzing its coupling to actomyosin-based activities in spatially confined areas in the cell cortex. We used manipulation of the intracel-

* This work was supported by Dutch Cancer Society Grant KUN 2002-1763. The costs of publication of this article were defrayed in part by the payment of page charges. This article must therefore be hereby marked "*advertisement*" in accordance with 18 U.S.C. Section 1734 solely to indicate this fact.

This work is dedicated to the memory of Wilma Peters.

[S] The on-line version of this article (available at http://www.jbc.org) contains supplemental Figs. S1–S3 and Movies 1–9.

† Deceased November 22, 2006.

[1] Both of these authors contributed equally to this work.

[2] Present address: N.V. Organon, Schering-Plough Corp., Dept. of Target Discovery, PO Box 20, 5340 BH Oss, The Netherlands.

[3] To whom correspondence should be addressed: Dept. of Cell Biology, Nijmegen Centre for Molecular Life Sciences, Radboud University Medical Centre, PO Box 9101, 6500 HB Nijmegen, The Netherlands. Tel.: 31-24-3614329; Fax: 31-24-3615317; E-mail: b.wieringa@ncmls.ru.nl.

lular positioning of the enzyme adenylate kinase-1 (AK1[4]; 2 ADP ↔ ATP + AMP (10, 11), also used as an ATP sensor in the literature (12)) as a tool to alter the intracellular landscape for ATP/ADP exchange and local fuelling by ATP. By testing the effects of different peripheral anchoring locations during cell motility, we provide new evidence for the idea that subcellular compartmentalization of ATP has an important role in cell shape control, presumably via regulation of local actomyosin behavior.

EXPERIMENTAL PROCEDURES

Cell Culture—Primary fibroblasts derived from 16.5 days post coitum mouse embryos (from wild type or AK1/CK-B double knock-out ($BAK^{-/-}$) strains) were immortalized poolwise using standard 3T3 cultivation protocols. Mouse embryonic fibroblasts (MEFs) and Phoenix (HEK293) packaging cells were cultured in Dulbecco's modified Eagle's medium (Invitrogen) supplemented with 4 mM glutamine, 2 mM sodium pyruvate, and 10% fetal calf serum.

Retroviral Constructs and Transfections—Mouse AK1, focal contact (FC)-targeted AK1 (EVH1-AK1), myristoylation-tagged AK1 (MYR-AK1), and YFP controls were expressed from recombinant inserts, cloned into EcoRI/XhoI sites of retroviral vector pLZRS-IRES-Zeo (13). To introduce location tags, we used PCR and primers with BamHI sites to generate a 345-bp segment from Ena-Vasp homology domain 1 (EVH1) from Mena (14) cDNA or a 50-bp myristoylation-domain segment from AK1β cDNA (15), respectively, and fused these 5′-upstream of DNA segments encoding Myc-tagged versions of AK1 and YFP. Location tags were 115 amino acids (EVH1) and 14 amino acids (MYR) long and carried their own ATG codons. To avoid ambiguity in translation initiation, natural start codons in the AK1 and YFP open reading frames were substituted by alanine codons. To study effects of inducible translocation of AK1, we used the ARGENT regulated heterodimerization kit (ARIAD Pharmaceuticals) based on rapamycin-induced heterodimerization of FKBP- and FRB-tagged proteins. The FKBP fragment (316 bp) from the pC4EN-F1 plasmid (ARIAD) was PCR-amplified, provided with EcoRI/XhoI sites, and cloned into the pLZRS-IRES-Zeo behind the EVH1-Myc sequence to generate the targeting construct. To generate the vector for FRB-tagged AK1, a 276-bp FRB fragment was PCR-amplified from plasmid pC4-RhE (ARIAD) template DNA with primers containing BamHI/BglII sites and cloned into the BamHI site upstream of the Myc-tagged AK1 sequence in vector pLZRS-IRES-Zeo. Constructs and targeting principle are depicted in Fig. 4, *A* and *B*. Integrity of all constructs was confirmed by DNA sequencing. To generate viral particles, Phoenix (HEK293) cells were grown on poly-L-lysine (10 μg/ml)-coated plates and transfected with retroviral pLZRS-IRES-Zeo constructs (5 μg) using Lipofectamine 2000 (10 μl; Invitrogen). After 8–16 h, medium with viral particles was harvested and filtered, Polybrene (5 μg/ml) was added, and the mixture was used to infect MEF-$BAK^{-/-}$. After 24 h, medium was replaced by medium containing zeocin (450 μg/ml; Invitrogen), and cells were kept under permanent selection for at least 2 weeks.

Western Blotting—SDS-PAGE and Western blotting analysis were performed using standard procedures. Primary or secondary antibodies used were polyclonal anti-AK1 serum (1:5000) (16), polyclonal anti-Myc serum (1:100, Developmental Studies Hybridoma Bank; University of Iowa), polyclonal anti-YFP (1:3000) (17) or anti-Tubulin (1:2000, Developmental Studies Hybridoma Bank; University of Iowa), and goat anti-mouse IRDye800 (Rockland) or goat anti-rabbit Alexa680 (Molecular Probes), respectively. Staining signals were detected using the Odyssey Imaging System (LI-COR Biosciences).

Immunofluorescence—Cells on coverslips were fixed, permeabilized, and stained as described (16). Primary and secondary antibodies used were polyclonal anti-AK1 (rabbit serum, 1:3000), anti-Myc (mouse serum, 1:5), or monoclonal anti-vinculin (1:500; Sigma) and goat-anti-mouse and goat anti-rabbit IgG-Alexa 488 or -Alexa 568 (1:500, Molecular Probes), respectively. F-actin was visualized with phalloidin-Alexa 660 (1:300; Molecular Probes). Samples were analyzed on an Axiophot2 (Carl Zeiss) or a DMRA (Leica) fluorescence microscope using ×63 and ×100 oil immersion objectives. Images were processed using Adobe Photoshop.

TIRF Microscopy—MEFs complemented with EVH1-YFP were trypsinized, resuspended in phenol red-free Dulbecco's modified Eagle's medium with serum and 1% fatty acid-free bovine serum albumin, and allowed to recover in suspension for 1 h at 37 °C. Subsequently, cells were plated on fibronectin (FN; 10 μg/ml)-coated WillCo dishes (WillCo Wells, Amsterdam, The Netherlands), and microscopic time lapse imaging was performed using an Olympus IX2 microscope equipped with a laser-based TIRFM module.

Cell Spreading Assay—Serum-starved cells were allowed to adhere and spread to FN-coated coverslips for 30 min, fixed in 2% paraformaldehyde, stained with phalloidin-Texas Red (1:300; Molecular Probes), and co-stained with antibodies against vinculin and AK1. Ten random fields were imaged per coverslip with a Bio-Rad confocal microscope MRC1024 using a ×10 objective. The total area covered after spreading was determined by Adobe Photoshop software, and the average surface occupied per cell was calculated. Spreading efficiencies were calculated using MEF-YFP cells as control.

Cell Migration Assays and Time Lapse Microscopy—Cell migration analysis was assessed as described elsewhere using FN (1 μg/ml)-coated coverslips (18). Prior to the monitoring, MEFs were starved for 4–24 h in Dulbecco's modified Eagle's medium containing 0.2% fetal calf serum and 5 mg/ml fatty acid-free bovine serum albumin before basic fibroblast growth factor (200 ng/ml; Peprotech) was added to stimulate migration. Time lapse imaging was done for 24 h in a microscope stage incubator (Oko-Lab) on a Nikon DiaPhot microscope equipped with a Hamamatsu C8484-05G digital camera. Images were taken every 10 min using TimeLapse Software (Oko-Lab), version 2.7, with a ×10 objective. Cells were tracked using Metamorph 6.1 measurement software (Universal Imag-

[4] The abbreviations used are: AK1, adenylate kinase-1; $BAK^{-/-}$, CK-B/AK1 double knock-out; CK-B, creatine kinase-B; EVH1, Ena-Vasp homology domain 1; FC, focal contact; FKBP, FK506 binding protein; FN, fibronectin; FRB, FKBP rapamycin-binding domain; MEF, mouse embryonic fibroblast; MYR, myristoylation domain; WT, wild type; YFP, yellow fluorescent protein.

ing Corp.) taking nuclei as reference. For each treatment, at least eight migrating cells of 3–5 independent assays were analyzed. The total track distance (*T*) and the direct distance from start to end point (*D*) were used to calculate *D*/*T* ratios reflecting the directionality of cell movements (19). Single cell motility assays were performed using an automated multiwell cell tracking system, as described (20).

AK Activity Assay—AK enzyme activity measurements were done as described (16).

ATP Measurements—Cellular ATP levels were measured using the luciferase-based CellTiter-Glo luminescent cell viability assay (Promega) according the manufacturer's protocol. 20,000–40,000 cells were lysed in freshly prepared CellTiter-Glo reagent, and ATP levels were calculated using an ATP standard curve. Luminescence was recorded using a LUMIstar Optima luminometer (BMG Labtech).

Rapalog-induced Repositioning of AK1—We used the chemical dimerization strategy based on heterodimerization of FKBP and FRB protein domains by rapalog (21) to reposition ATP/ADP exchange capacity in the cell. MEF-BAK$^{-/-}$, stably transfected with EVH1-FKBP and empty MEF-BAK$^{-/-}$ cells (control), were retrovirally transduced with FRB-AK1 and directly (passages 2–8) used for motility and immunofluorescence studies. Rapalog-treated (200 nM; ARIAD) and nontreated cells were analyzed for subcellular positioning of AK1, and cell migration was monitored.

Statistics—Data are presented as the mean ± S.E. of 3–6 independent experiments. Groups were compared with Student's *t* test for single values, ratio *t* test for ratio values, and one-sample *t* test for relative values and considered significantly different when p was <0.05.

RESULTS

Expression and Localization of (Targeted) AK1 in MEFs—MEFs derived from BAK$^{-/-}$ mice were used to generate cell lines expressing nontargeted (cytosolic), FC-targeted, and membrane-targeted AK1. The BAK$^{-/-}$ background was chosen, because AK1- and CK-B-catalyzed reactions share ATP-generating capacity and thus show redundancy in function. AK1 and CK-B are the only members of their respective families occurring at detectable levels in the cytosol of WT MEFs. Here we restricted ourselves to the analysis of the role of AK1 alone. Transduction of MEF-BAK$^{-/-}$ cells with retroviral expression vectors for the different AK1 variants or YFP controls (Fig. 1*A*) yielded pools of cells that were designated MEF-AK1, MEF-EVH1-AK1, or MEF-MYR-AK1. As shown by Western blot analysis (Fig. 1*B*), proteins of the correct size were produced, at expression levels of EVH1- and MYR-tagged AK1 that were roughly 2–3 times higher than that of endogenous AK1 in WT MEFs. Only in MEF-EVH1-AK1 cells an additional truncated extra protein was produced, but we know that this product results from use of an internal ATG start codon within the EVH1 sequence. Because the majority of the AK1 molecules appeared as a tagged form, no further action was taken on this point. For the YFP controls, we noted a lower expression of the EVH1-YFP variant compared with the nontargeted and MYR-YFP protein (Fig. 1*B*).

Enzymatic activity assays (Fig. 1*C*) revealed that the total ATP-generating capacity in cells with EVH1- or MYR-tagged AK1 variants was lower than in MEF-AK1 but considerably higher than in MEF-YFP controls. Activity was completely inhibited by Ap5A, a potent AK inhibitor. Of note, the total cellular ATP level remained virtually unchanged upon complementation with WT or tagged AK1 and was determined at 0.025 ± 0.013 pmol/cell for MEF-BAK$^{-/-}$ cells and at 0.018 ± 0.012, 0.017 ± 0.009, and 0.015 ± 0.004 pmol/cell for MEF-AK1, MEF-EVH1-AK1, and MEF-MYR-AK1 cells, respectively (values of three independent experiments ± S.D.; no significant differences). In hindsight this is not a surprising finding, since the role of AK is in ADP-ATP exchange and the setting of the cell's energy charge does not necessarily change upon transfection of cells in culture.

AK1 is reported to be a monomeric cytosolic protein, which also occurs in trace amounts on nuclear and vesicular membranes (22). Indeed, in our retrovirally transduced cells, we found AK1 (like the YFP control) smoothly distributed across the cytosol, with an apparent concentration around nuclei, close to membranes of the Golgi compartment (Fig. 1, *D* and *E*). For EVH1-AK1 and EVH1-YFP, we found, besides a cytosolic localization, a strong accumulation at structures resembling FC (Fig. 1, *D* and *E*), where these proteins co-localized with vinculin (Fig. 1, *F* and *G*). Strikingly, for EVH1-AK1, co-localization was mostly observed in the cell periphery, whereas we also found FC that stained positive for vinculin only (Fig. 1*F*). For EVH1-YFP, we observed some FC that stained mutually exclusively for YFP or vinculin (Fig. 1*G*). Only a small fraction of EVH1-protein decorated FC at any given time point. As anticipated, (re)addition of the AK1β-derived MYR tag drove proteins into membrane anchoring, exactly as reported for the natural variant (15, 16). Both MYR-AK1 and MYR-YFP showed a punctuate distribution pattern, with protein decorating vesicular and plasma membranes (Fig. 1, *D* and *E*). Live imaging of MEF-MYR-YFP cells confirmed that the small cluster-like structures represent (mobile) vesicles (data not shown).

Dynamics of EVH1 Targeting during Cell Spreading—To obtain an in depth picture for timing of targeting, we analyzed MEF-EVH1-YFP cells during adherence to FN with TIRF microscopy. During early spreading (20 min), EVH1-YFP appeared in dotlike structures, which were preferentially located at the cell periphery (Fig. 2*A*, *arrowheads*), resembling immature FC, also known as spreading initiation centers (23). Mature focal adhesions with a more elongated shape were abundantly present at 120 min (Fig. 2*B*, arrows). Maturation of dotlike structures into elongated FC was followed by video recording (Fig. 2*C* and supplemental Movie 1). Our data show that fusing proteins to the EVH1 domain results in effective targeting to FC during cell spreading, with apparently no detrimental effects on the spreading process proper. We conclude that our strategy of deliberate swapping of cellular positioning of AK1 forms a reliable basis to study effects of spatial rewiring of ATP/ADP supply capacity.

ATP/ADP Exchange Capacity Determines Cell Spreading—To assess the functional-modulatory effects of changes in local ATP supply on cytoskeletal behavior, we first tested adherence-spreading ability of the different cells. Comparison of spreading ability revealed no differences between MEF-AK1 and MEF-YFP (Fig. 2, *D* and *E*). Interestingly, for cells with targeted AK1, we found that expression of EVH1-AK1, but not MYR-AK1,

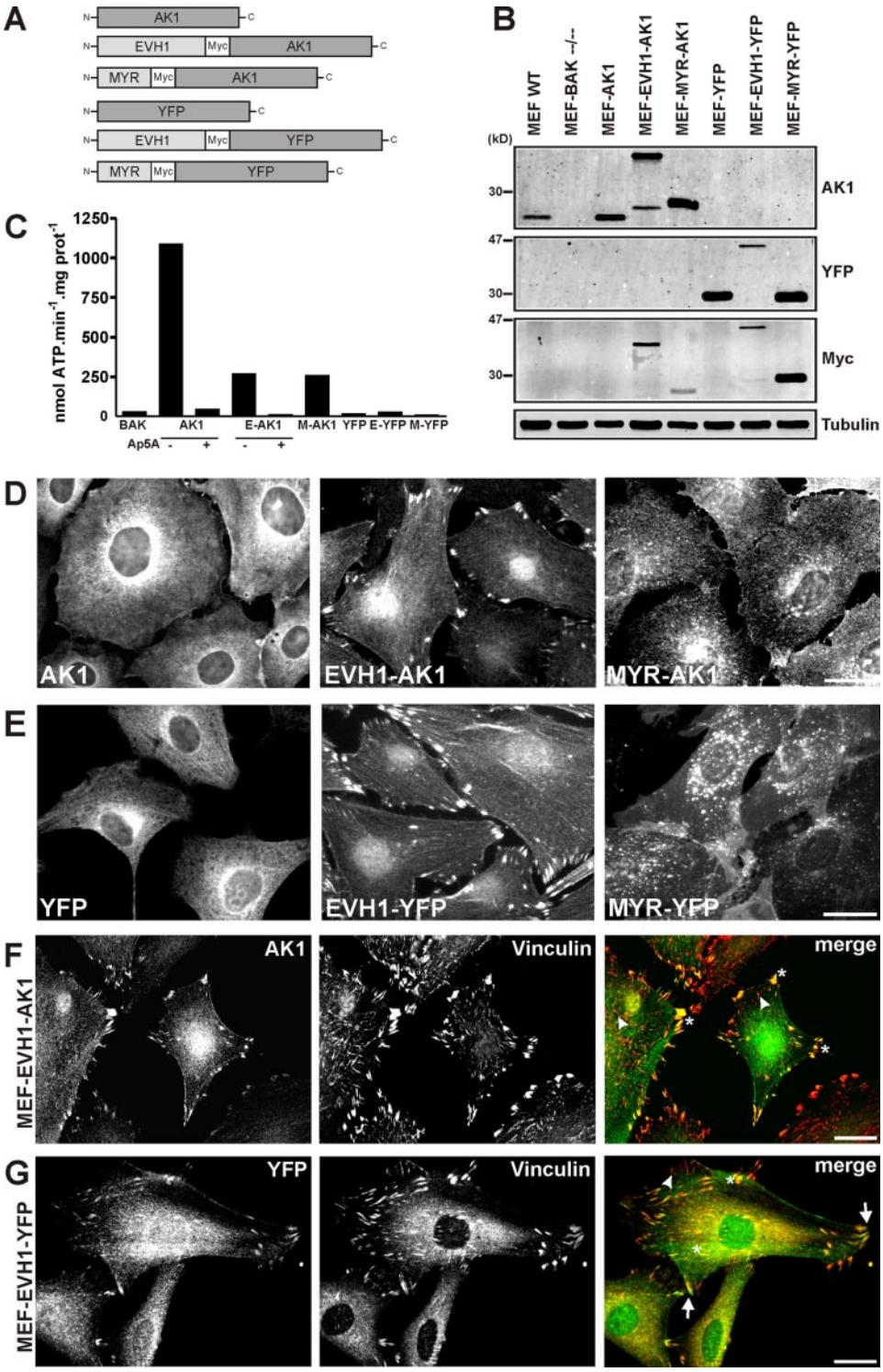

FIGURE 1. **Cellular distribution of untagged *versus* tagged AK1 and YFP.** *A*, schematic representation (not drawn to scale) of the constructs used to complement MEF-BAK$^{-/-}$ cells. *B*, Western blotting of lysates of WT MEF- and MEF-BAK$^{-/-}$-expressing AK1, tagged AK1, or YFP variants. AK1 is expressed in WT MEF and all AK1-complemented cells. Myc signals were used to compare the expression of tagged AK1 and YFP. Tubulin was used as loading control. *C*, AK-specific enzyme activity is increased in lysates of MEF-AK1, MEF-EVH1-AK1, and MEF-MYR-AK1, compared with YFP variants. Note that AK activity is absent in MEF-BAK$^{-/-}$ and blocked in the presence of the specific inhibitor Ap5a (50 μM). *D* and *E*, immunofluorescence using antibodies against AK1 (*D*) or direct fluorescence detection of YFP (*E*) shows a cytoplasmic localization for AK1 and YFP, accumulation at FC for EVH1-AK1 and EVH1-YFP, and staining of membranes and internal vesicles for cells expressing MYR-AK1 or MYR-YFP. *Bar*, 20 μm. *F* and *G*, EVH1 targeting of AK1 and YFP results in targeting to vinculin-positive adhesions. The *asterisks* indicate co-localization. Nontargeted adhesions (*arrowhead*) and FC positive for YFP and vinculin without complete co-localization (*arrow*) are indicated. *Bar*, 20 μm.

induced a small but significant (p = 0.0357, n = 4) increase of ~25% in the area over which spreading occurred. Targeting of EVH1-AK1 during spreading proceeded as anticipated, as confirmed by staining for AK1 and vinculin (Fig. S1). These findings suggest that the ATP/ADP exchange activity of AK1, when brought to spatially restricted areas in the cell cortex, codetermines spreading behavior.

ATP/ADP Exchange Capacity Determines Cell Motility—To study other effects of changes in local ATP/ADP on cell behavior, we used the barrier assay for cell motility analysis (18). Interestingly, all AK1-complemented MEFs showed significant increased migration as compared with YFP controls (Fig. 3*A*). Highest stimulation of motility was observed in MEF-EVH1-AK1 cells (~530 μm in 24 h; Fig. 3*A*). Also for MEF-MYR-AK1 cells, the increase in motility compared with MEF-AK1, was significant. Experiments using conventional single cell motility assays confirmed the activating effect of EVH1-AK1, although effects were less evident (Fig. S2). All YFP control cells behaved comparably, with migration distances around 250 μm (Fig. 3*A*). Directionality of cell movements was slightly higher for MEF-EVH1-AK1 (Fig. 3*B*). Migration morphology revealed minor differences (Fig. 3, *C* and *D*, and supplemental Movies 2–7). Consistently, MYR-targeted cells appeared somewhat bigger in culture.

Still images of fixed cells, captured at different phases in the cyclic motility process, revealed that the typical AK1 distribution patterns with cytosolic, FC, or membrane accumulation were globally preserved for all complemented MEF but that variation in enzyme location occurred during motility (Fig. S3, *A*–*C*). For example, in MEF-EVH1-AK1 cells, dotlike foci in leading edges were seen, resembling newly formed FC, and AK1 staining in mature FC disappeared over time (Fig. S3*B*). Importantly, co-staining experiments with phal-

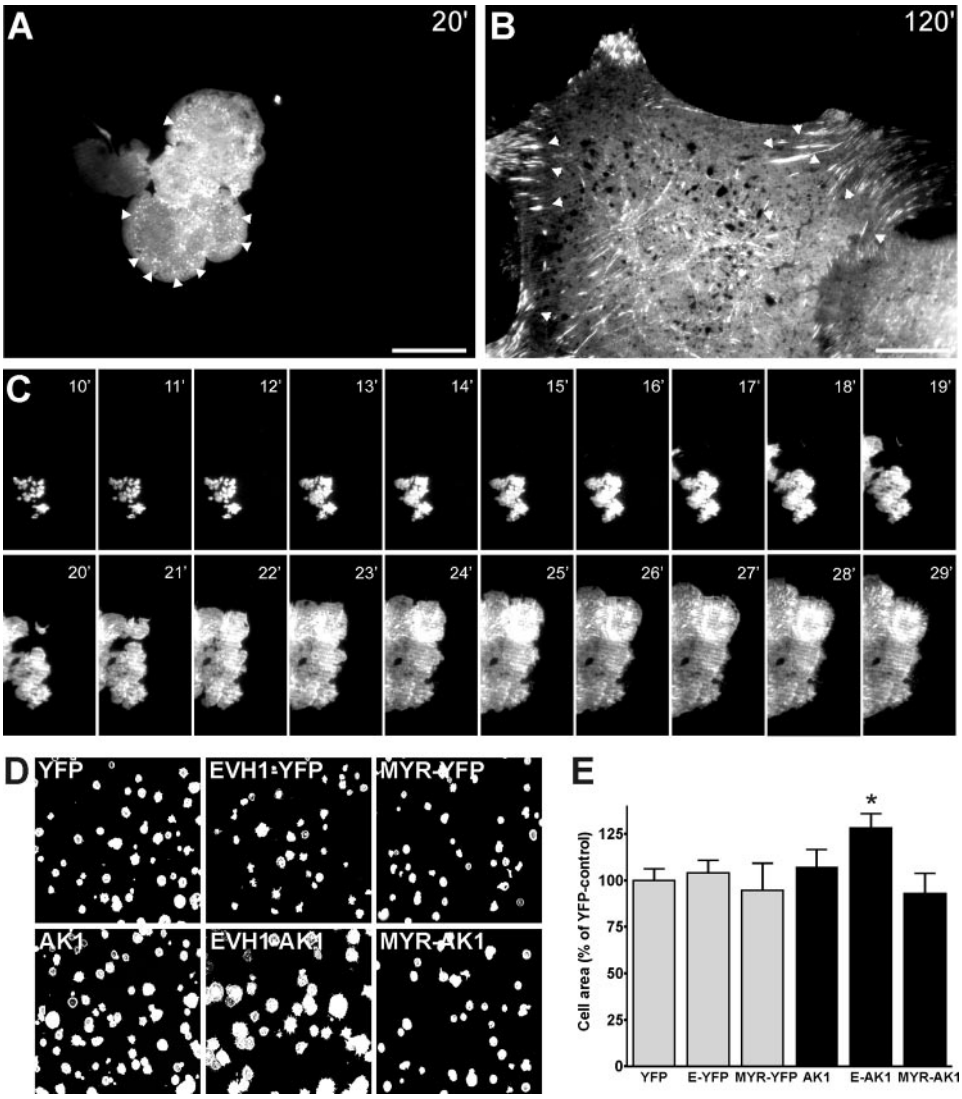

FIGURE 2. **Cell spreading efficiency is increased by FC-targeted AK1.** *A* and *B*, TIRF microscopy of MEF-EVH1-YFP cells after spreading for 20 min (*A*) or 120 min (*B*) on FN. The *still pictures* reveal YFP-positive focal contacts with a rounded, immature appearance (20 min; *arrowheads*) and with an elongated morphology after 120 min (*arrowheads*). *Bar*, 10 μm. *C*, time series of a representative TIRF movie (see also supplemental Movie 1) of a spreading MEF-EVH1-YFP cell. Note the formation and maturation of YFP-positive focal contacts. *D* and *E*, quantitative cell spreading assay. MEF cells were allowed to spread for 30 min, fixed, phalloidin-stained, and photographed. Areas occupied by cells were calculated by processing of the binary images as described under "Experimental Procedures." MEF-EVH1-AK1 cells have increased spreading capacity as compared with YFP controls (*, $p < 0.05$).

loidin revealed that AK1 never co-localized with static F-actin in stress fibers (Fig. S3*D*). Instead, EVH1-AK1 remained concentrated at cell peripheral endings of stress fibers, where the more dynamic actin resides. MYR-AK1 was mainly located at the rim of the leading edge shortly after migration induction. AK1 and MYR-AK1 also locally accumulated in intracellular vesicles, at the cell periphery and retracting tails (Fig. S3, *asterisks*).

Effects of Inducible Translocation of ATP/ADP Exchange Capacity on Cell Motility—To obtain better control over background variation in global ATP/ADP exchange activity and the time frame in which the effects of (re)location of AK1 can be induced, we next used rapamycin-analog (rapalog)-mediated heterodimerization of FRB (domain of mTOR that binds FKBP12) and FKBP12 (FK506-binding protein) to transiently translocate AK1 (21). Effects of shifting AK1 location were studied for the EVH1 derivative only, the location tag that gave the most prominent effects in previous experiments. To create host cells with an acceptor-destination target, $BAK^{-/-}$ cells were first transduced with a retroviral vector encoding an EVH1-FKBP12 fusion protein. These host cells were infected again, now with FRB-AK1. Constructs and concept are shown in Fig. 4, *A* and *B*. Comparison of immunofluorescent staining patterns before and after the addition of rapalog revealed that our experimental design was successful, because a substantial fraction of FRB-AK1 molecules translocated from the cytosol to FC-located EVH1-FKBP partners (Fig. 4*C*, *arrows*). This inducible repositioning of FRB-AK1 in MEF-EVH1-FKBP cells had a strong effect on migration distance, as demonstrated by the significant increase in migratory activity in 24 h ($p = 0.0009$, $n = 4$; Fig. 4, *D* and *E*). Strikingly, migration distances observed in cells with and without rapalog accurately overlapped with those of MEF-AK1 and MEF-EVH1-AK1 (see Fig. 3*A*). Since by this set of experiments we have managed to uncouple effects of enzyme level and activity from effects of enzyme location, we conclude that (re)positioning of the ATP/ADP exchange capacity indeed forms a distinct condition that, among others, determines the motility properties of cells.

DISCUSSION

Experimental Model System—To design a new experimental setting for the study of coupling between local ATP supply and cell dynamics, we developed a transfection complementation strategy with AK1 fusion proteins in MEFs derived from $BAK^{-/-}$) mice. Both AK1 and CK-B are principal enzymes for offering fuel-demanding systems access to locally produced ATP (10, 24), and their removal therefore gave us the opportunity to study effects of redistribution of enzymatic ATP/ADP exchange capacity without background effects. To achieve altered distribution patterning over cytosol and cell cortical areas, we provided AK1 (or YFP controls) with an N-terminal tag from the EVH1 domain of Mena, a protein known to local-

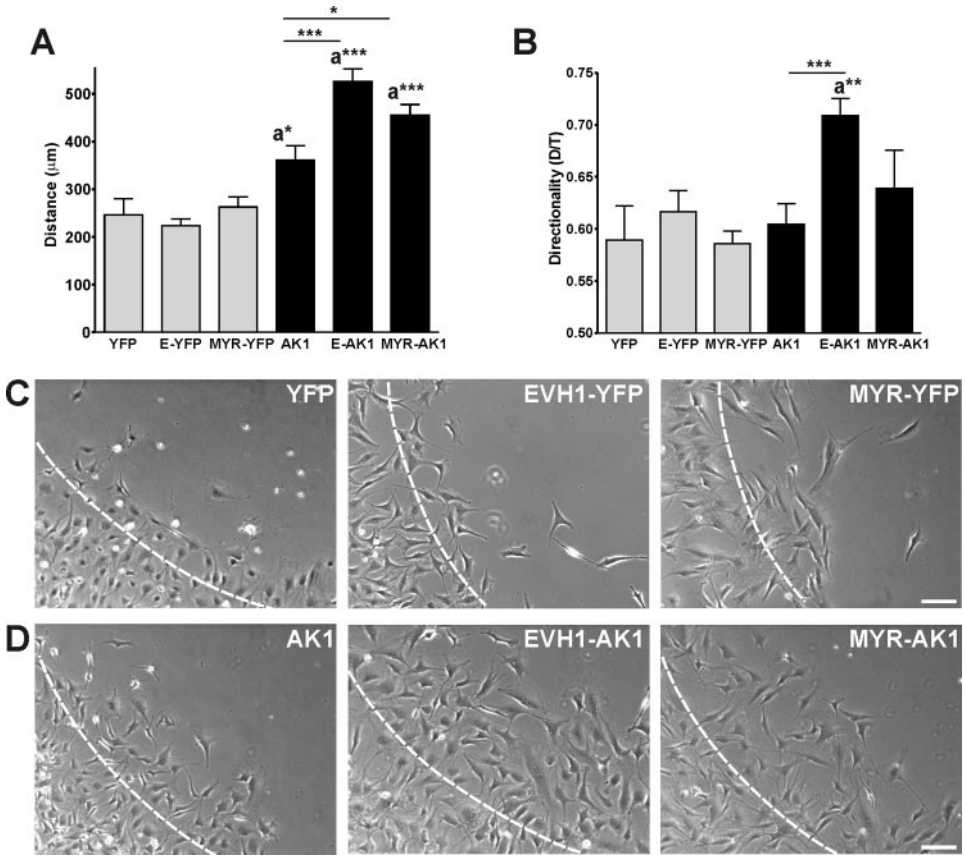

FIGURE 3. **Forced subcellular expression of AK1 increases cell motility.** *A* and *B*, quantification of migratory activity. Average migration distances. Note that MEF-AK1, MEF-EVH1-AK1, and MEF-MYR-AK1 cells have significantly higher migratory capacities than YFP controls (*A*). Migratory directionality of cells from YFP- and AK1-complemented MEF is plotted (*B*). Note that MEF-EVH1-AK1 are significantly different from MEF-AK1 and MEF-EVH1-YFP controls (*, $p < 0.05$; **, $p < 0.01$; ***, $p < 0.001$). *C* and *D*, morphology of migrating YFP (*C*) and AK1 (*D*)-expressing MEFs during migration in the barrier assay. Shown are representative images of migrating cells after 24 h obtained from migration movies (supplemental Movies 2–7). The *dashed lines* indicate migration front at 0 h. *Bar*, 100 μm.

ize at filopodial tips, leading edges, and FC (14) or with a MYR sequence derived from a known natural isoform of AK1, AK1β (16). The EVH1 domain was chosen, because FCs are known as centers of high local actin polymerization activity during assembly, maturation, and disassembly of adhesion (de)formation (25). Use of the MYR domain as tag would allow us to bring the ATP supply capacity of AK1 into a near membrane position. Both tags drive ATP supply close to regions of cortical actomyosin activity needed for membrane protrusion and cell migratory activity. Our localization studies confirmed that cellular redistribution indeed occurred as anticipated but also pointed out that the EVH1-driven recruitment involves only a relatively small fraction of the total pool of AK1 molecules present at any point in time. Moreover, for EVH1-AK1 and EVH1-YFP, we noticed that not all FC sites are targeted simultaneously. These observations can be explained by the highly dynamic nature of adhesion structures in migrating cells (26). Additionally, the quantity of EVH1-tagged molecules in our cells may simply oversaturate the amount of locally available binding motifs in FC proteins like vinculin and zyxin. Likewise, also MYR tagging did not result in guidance of all AK1 molecules to plasma membrane locations only. A considerable portion of AK1 appeared anchored to intracellular membranes in all cell images examined. Importantly, we also found that N-terminal tagging rendered the enzymatic capacity of AK1 less active (*in vitro* experiments confirmed that the specific activity of recombinant AK1s, expressed as arbitrary units/mg of protein was 2–4-fold lowered; data not shown).

Together, these data demonstrate that (i) terminal juxtaposition of EVH1 and MYR domains is compatible with AK1 activity but that global ATP/ADP exchange capacity is on average highest in the cell pool with WT AK1, and (ii) tagging helped us to establish an experimental cell model in which a relatively small portion of the total ATP/ADP exchange capacity is effectively redirected to new cell-cortical locations. Although we cannot exactly quantify this fraction due to its dynamic character, these findings make it highly unlikely that any differential effects on cell spreading and motility are attributable to variations in global ATP supply capacity between cell pools. Also, variation in overall cellular ATP level in different transfected cell pools was negligible and cannot explain our findings. We consider these strong arguments in support of the validity of our model system and strategy for read-out of positional effects of ATP supply capacity.

Local ATP/ADP Exchange Enhances Cell Spreading—MEF-EVH1-AK1 cells showed an increased capacity to spread out on FN matrixes. Expression of AK1 or MYR-AK1 did not result in more effective cell spreading compared with YFP control cells. Cell-to-substrate attachment and early spreading are passive events, which appear universal for many cell types over a wide range of substrates (27, 28). Later events in spreading may be more reliant on infrastructural organization within the cell and be cell type-dependent. Together, adherence and spreading can be considered a "relatively mild cellular exercise." These system properties may attribute to the fact that we only see measurable effect of addition of ATP supply machinery on cell spreading if we manage to direct its capacity to direct relevant niches in the cell (*i.e.* as in the case of MEF-EVH1-AK1 cells). Moreover, because MEF-EVH1-AK1 cells show increased cell spreading capacity, we conclude that subcellular location of ATP supply capacity in isolation from the mere presence of overall capacity is a specific parameter.

Local ATP/ADP Exchange Enhances Cell Motility—Migratory capacity of fibroblasts was enhanced in all types of AK1-complemented cells (cytosolic and targeted) as demonstrated by increased migration distance compared with YFP control

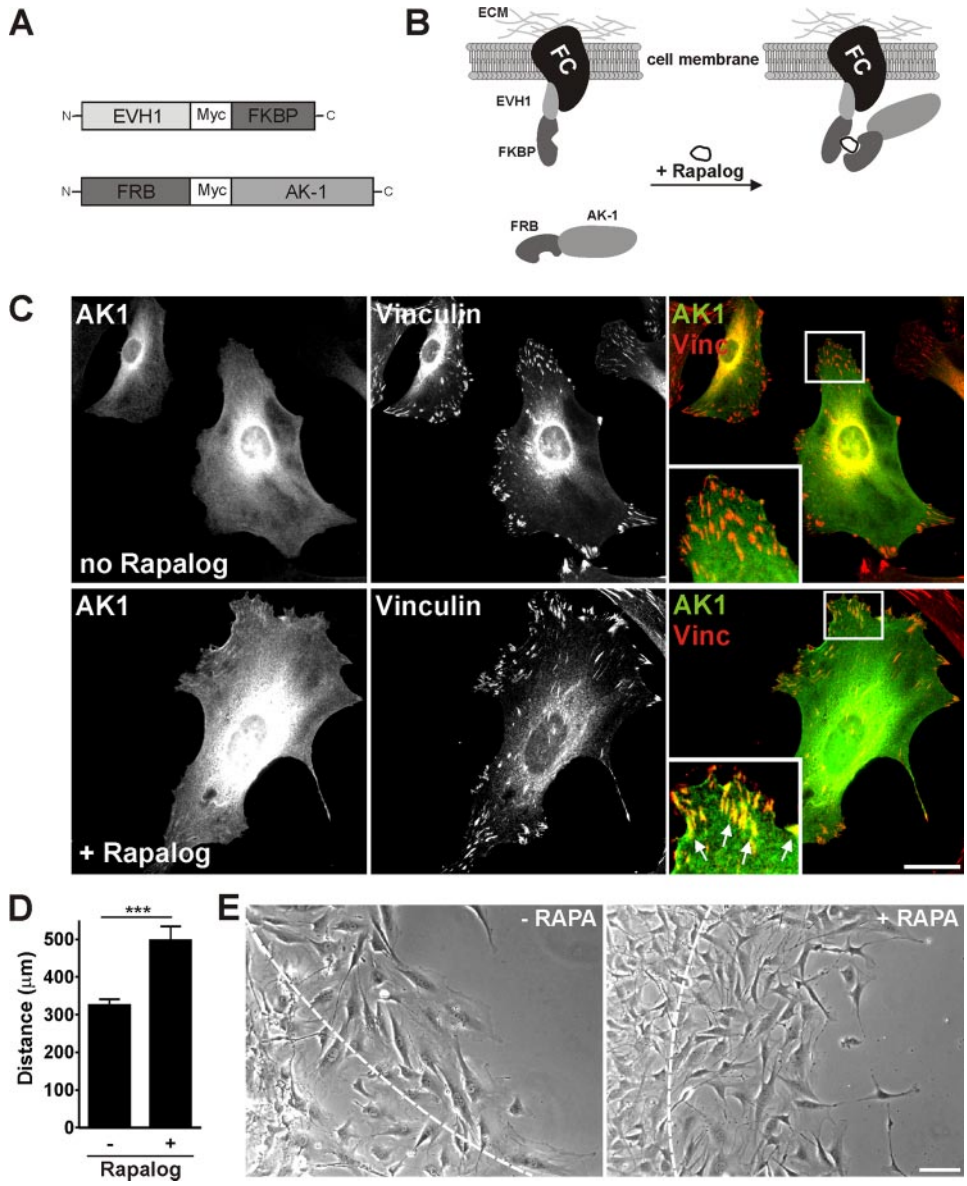

FIGURE 4. **Rapalog-induced repositioning of AK1 stimulates migration.** *A*, schematic representation of constructs used for expression of EVH1-tagged FKBP and FRB-tagged AK1 partner proteins, not drawn to scale. *B*, scheme of rapalog-induced heterodimerization of EVH1-FKBP with cytosolic FRB-AK1. Binding of FKBP to FRB moieties results in a change in local ATP/ADP via repositioning of AK1 to FC. *C*, MEF-BAK$^{-/-}$ cells stably expressing EVH1-FKBP were retrovirally transduced with FRB-AK1. Shown are images of fixed cells stained for AK1 and vinculin, before and 1 h after the addition of rapalog. Note that rapalog induces repositioning of AK1 from cytosol to FC within 1 h. The *insets* show AK1/vinculin co-staining at the cell periphery. Without rapalog, all adhesions stained *red* (vinculin positive only), whereas after the rapalog addition, many FC show co-localization (*arrows*). *Bar*, 20 μm. *D*, EVH1-FKBP- and FRB-AK1-expressing cells were allowed to migrate along FN in the presence or absence of rapalog. The addition of rapalog resulted in a significant increased migrated distance (***, $p < 0.001$). *E*, morphology of migrating cells after 24 h of migration in the absence or presence of rapalog (*RAPA*; *pictures* obtained from supplemental Movies 8 and 9). The *dashed lines* indicate migration front at 0 h. *Bar*, 100 μm.

cells (depicted with *a* in Fig. 3*A*). Most simply this finding can be explained by the fact that cell movement is a more energy-demanding activity than cell spreading (28), and as a consequence, the threshold for adequate ATP fuelling becomes more reliant on global ATP/ADP exchange capacity. Even more importantly, we observed that MEF-EVH1-AK1 cells were most migratory among AK1-complemented cells. Apparently, protein position effects appear dominant over concentration effects in this case, because overall enzymatic AK1 activity in MEF-AK1 was more than 3 times higher than in MEF-EVH1-AK1 or MEF-MYR-AK1, but migratory changes were more evident in the latter two cell pools. The fact that the most prominent stimulation was induced by EVH1 targeting, with only a relatively small fraction of the total pool of active cellular enzyme recruited into FC, further supports the idea that patterning in ATP-distribution matters.

The third and strongest indication in support of relevance of "ATP/ADP compartmentation" comes from the experiments with transient spatial redistribution of AK1-mediated ATP/ADP exchange capacity in the same cell pools (Fig. 4). Upon translocation of (a fraction of) the intracellular AK1 pool toward FC, migratory capacity of fibroblasts was immediately significantly induced. We know that only intracellular metabolic effects have to be considered, because the addition of apyrase to intact cells had no effects on migratory behavior (not shown). Therefore, a promoting role for formation of extracellular ATP (12) acting as an attractant chemokine as described for neutrophils (29, 30) can be excluded.

Based on all evidence combined, we propose that our FC- or membrane-targeted AK1 serves in areas with restricted diffusion of ATP (similar to that found for AK in flagella (31)) and that the enzyme's role in providing ATP for cytoskeletal dynamics forms the most direct link. During motility, cells transiently form protruding filopodia and lamellipodia in multiple dimensions, for which ATP-dependent actin polymerization and myosin ATPase activity are the principal driving forces (32, 33). For neurons, it is known that ATP hydrolysis required for actomyosin remodeling may account for up to 50% of global cellular energy consumption (6), and we may now have to think of this in terms of integrated ATP use at multiple cellular sites. Our own recent studies on cells derived from our animal models without phosphotransfer (*i.e.* ATP supply) capacity and RAW macrophages support the important role of on site ATP fuelling (9). Whether we must explain our findings on the effects of local arrest of AK1 either by the enzyme's role in direct ATP/ADP exchange or perhaps by facilitating

"release" of ATP from intramolecular stacking interactions, in spatially confined microcompartments of the cell, is a subject for further study.

In summary, findings with our experimental models for spatial repositioning of AK1 provide circumstantial evidence for a regulatory role of ATP compartmentation in actin cytoskeletal dynamics in microdomains of the cell. Further study with development of sensors for readout of intracellular [ATP] distribution (34) will be required to delineate how the cellular energy landscape determines cytoskeleton dynamics. Broadening of studies to other cell types and other ATP supply systems may ultimately help to provide more insight into how local [ATP]/[ADP] controls cell shape changes. Such studies may also help to disclose new possibilities for metabolic control of metastatic potential of tumor cells.

Acknowledgment—We thank Rinske van de Vorstenbosch for assistance in several cloning experiments.

REFERENCES

1. Balaban, R. S. (1990) *Am. J. Physiol.* **258,** C377–C389
2. Chhabra, E. S., and Higgs, H. N. (2007) *Nat. Cell Biol.* **9,** 1110–1121
3. Pollard, T. D., and Borisy, G. G. (2003) *Cell* **112,** 453–465
4. Volkmann, N., and Hanein, D. (2000) *Curr. Opin. Cell Biol.* **12,** 26–34
5. Etienne-Manneville, S., and Hall, A. (2002) *Nature* **420,** 629–635
6. Bernstein, B. W., and Bamburg, J. R. (2003) *J. Neurosci.* **23,** 1–6
7. Gourlay, C. W., and Ayscough, K. R. (2005) *Nat. Rev. Mol. Cell. Biol.* **6,** 583–589
8. Ueda, T., Mori, Y., and Kobatake, Y. (1987) *Exp. Cell Res.* **169,** 191–201
9. Kuiper, J. W., Pluk, H., Oerlemans, F., van Leeuwen, F. N., de Lange, F., Fransen, J., and Wieringa, B. (2008) *PLoS Biol.* **6,** e51
10. Janssen, E., Dzeja, P. P., Oerlemans, F., Simonetti, A. W., Heerschap, A., de Haan, A., Rush, P. S., Terjung, R. R., Wieringa, B., and Terzic, A. (2000) *EMBO J.* **19,** 6371–6381
11. Noda, L. H. (1973) in *The Enzymes* (Boyer, P. D., ed) pp. 297–305, Academic Press, Inc., New York
12. Yegutkin, G. G., Mikhailov, A., Samburski, S. S., and Jalkanen, S. (2006) *Mol. Biol. Cell* **17,** 3378–3385
13. Michiels, F., van der Kammen, R. A., Janssen, L., Nolan, G., and Collard, J. G. (2000) *Methods Enzymol.* **325,** 295–302
14. Gertler, F. B., Niebuhr, K., Reinhard, M., Wehland, J., and Soriano, P. (1996) *Cell* **87,** 227–239
15. Collavin, L., Lazarevic, D., Utrera, R., Marzinotto, S., Monte, M., and Schneider, C. (1999) *Oncogene* **18,** 5879–5888
16. Janssen, E., Kuiper, J., Hodgson, D., Zingman, L. V., Alekseev, A. E., Terzic, A., and Wieringa, B. (2004) *Mol. Cell Biochem.* **256,** 59–72
17. Cuppen, E., Wijers, M., Schepens, J., Fransen, J., Wieringa, B., and Hendriks, W. (1999) *J. Cell Sci.* **112,** 3299–3308
18. Van Horssen, R., Galjart, N., Rens, J. A., Eggermont, A. M., and ten Hagen, T. L. (2006) *J. Cell. Biochem.* **99,** 1536–1552
19. Pankov, R., Endo, Y., Even-Ram, S., Araki, M., Clark, K., Cukierman, E., Matsumoto, K., and Yamada, K. M. (2005) *J. Cell Biol.* **170,** 793–802
20. Krooshoop, D. J., Torensma, R., van den Bosch, G. J., Nelissen, J. M., Figdor, C. G., Raymakers, R. A., and Boezeman, J. B. (2003) *J. Immunol. Methods* **280,** 89–102
21. Castellano, F., Montcourrier, P., Guillemot, J. C., Gouin, E., Machesky, L., Cossart, P., and Chavrier, P. (1999) *Curr. Biol.* **9,** 351–360
22. Ruan, Q., Chen, Y., Gratton, E., Glaser, M., and Mantulin, W. W. (2002) *Biophys. J.* **83,** 3177–3187
23. de Hoog, C. L., Foster, L. J., and Mann, M. (2004) *Cell* **117,** 649–662
24. van Deursen, J., Heerschap, A., Oerlemans, F., Ruitenbeek, W., Jap, P., ter Laak, H., and Wieringa, B. (1993) *Cell* **74,** 621–631
25. Choi, C. K., Vicente-Manzanares, M., Zareno, J., Whitmore, L. A., Mogilner, A., and Horwitz, A. R. (2008) *Nat. Cell Biol.* **10,** 1039–1050
26. Webb, D. J., Parsons, J. T., and Horwitz, A. F. (2002) *Nat Cell Biol.* **4,** E97–E100
27. Bereiter-Hahn, J., Luck, M., Miebach, T., Stelzer, H. K., and Voth, M. (1990) *J. Cell Sci.* **96,** 171–188
28. Cuvelier, D., Thery, M., Chu, Y. S., Dufour, S., Thiery, J. P., Bornens, M., Nassoy, P., and Mahadevan, L. (2007) *Curr. Biol.* **17,** 694–699
29. Chen, Y., Corriden, R., Inoue, Y., Yip, L., Hashiguchi, N., Zinkernagel, A., Nizet, V., Insel, P. A., and Junger, W. G. (2006) *Science* **314,** 1792–1795
30. Corriden, R., Chen, Y., Inoue, Y., Beldi, G., Robson, S., Insel, P. A., and Junger, W. G. (2008) *J. Biol. Chem.* **283,** 28480–28486
31. Ginger, M. L., Ngazoa, E. S., Pereira, C. A., Pullen, T. J., Kabiri, M., Becker, K., Gull, K., and Steverding, D. (2005) *J. Biol. Chem.* **280,** 11781–11789
32. Tokuo, H., Mabuchi, K., and Ikebe, M. (2007) *J. Cell Biol.* **179,** 229–238
33. Romero, S., Didry, D., Larquet, E., Boisset, N., Pantaloni, D., and Carlier, M. F. (2007) *J. Biol. Chem.* **282,** 8435–8445
34. Willemse, M., Janssen, E., de Lange, F., Wieringa, B., and Fransen, J. (2007) *Nat. Biotechnol.* **25,** 170–172